

Distribution of lateral active earth pressure on a rigid retaining wall under various motion modes

Negar Salehi Alamdari ^a, Mohammad Hossein Khosravi ^{b, *}, Hooshang Katebi ^a

^a Department of Geotechnical Engineering, Faculty of Civil Engineering, University of Tabriz, Tabriz, Iran

^b School of Mining Engineering, College of Engineering, University of Tehran, Tehran, Iran

Article History:

Received: 13 May 2019,

Revised: 21 September 2019

Accepted: 21 September 2019.

ABSTRACT

The design of retaining walls depends on the magnitude of active pressure exerted from the backfill. Therefore, estimating the scale of this pressure is a fundamental factor in the design. In this study, to assess the active earth pressure, a rigid retaining wall was built capable of translating and/or rotating with adjustable speed. Further, several physical tests were conducted on a laboratory scale under the influence of uniform surcharge. In order to evaluate the behavior of the soil and the failure wedge, circular flat pressure cells and particle image velocimetry method were used. The results indicated that in the translation and translation-rotational modes, the distribution of lateral active pressure along the wall height was non-linear while it was relatively linear under rotation around the base. By increasing the amount of surcharge, the effect of the arching phenomenon at the lower portion of the wall was more evident. This led to a negligible magnitude of pressure at the base of the wall. In addition, it was observed that during the active motion of the wall, the distinction between the stationary region and the failure zone was a function of the mode of wall motion.

Keywords : Active earth pressure, rigid retaining wall, rotation mode, translation mode

1. Introduction

The design of a retaining wall depends on the amount of active pressure exerted from the backfill. Therefore, estimating the amount of active pressure exerted on a rigid retaining wall is a major factor in the design process. Accordingly, many efforts have been made to evaluate the behavior of the retained backfill via physical and numerical modeling as well as theoretical analyses. Conventionally, Coulomb's and Rankine's methods [1,2] are used to calculate the active pressure behind rigid retaining walls. The arching phenomenon was first investigated based on the events occurring in silos, where Janssen's theory [3] was raised to estimate the lateral pressure in silo walls. Terzaghi [4] predicted that the failure plane occurring behind the wall was of parabolic type, and the maximum pressure did not occur at the base of the wall. He attributed these observations to the arching effect. Following Janssen's theory and Terzaghi's studies, extensive research studies have been conducted to develop this theory and to study the arching effect across various engineering fields such as retaining walls, tunnels, piles, stone column-supported embankments, and pipelines. Physical tests and numerical analyses on retaining walls indicated that the distribution of active pressure behind the wall is non-linear and is influenced by the arching effect [5-10]. In recent years, due to the complexity of the problem, other researchers have tried to investigate the influence of arching phenomena on the lateral earth pressure. Paik and Salgado [5] proposed a formulation for calculating the active earth pressure while considering the arching effect. However, the effect of surcharge pressure on the amount of lateral pressure was not considered in these studies. Pipatpongsa and Heng [11] analytically investigated the silo effect under the influence of uniform vertical pressure and the

formation of arch shapes in granular materials. Based on these studies, an assumption of uniform vertical stress in Janssen's classical theory corresponds to the assumption of a linear reduction of shear stress based on Jaky's approach [12]. Khosravi et al. [9, 13] conducted an analytical study on a rigid retaining wall system under active horizontal translation movement with a uniform surcharge on the retained backfill. Unlike previous works conducted in this field, the analyses were carried out in a two-dimensional system of equilibrium in rectangular coordinates. A new formulation was proposed to evaluate the magnitude and distribution of vertical, lateral, and shear stresses in the failure zone behind a retaining wall. These theories were later developed for the assumption of a nonlinear failure surface behind the wall [14].

In addition to analytical methods, physical modeling and experiments have also been performed to analyze the pressure of the soil behind the retaining wall and to test the arching effect in granular materials. Khosravi [9, 15] conducted several physical tests to determine the active earth pressure behind a rigid retaining wall under the translation mode without considering the surcharge effect. A good agreement between the experimental results and the predictions derived from the proposed formulation considering the arching effect confirmed such a phenomenon behind the wall. The influence of wall face friction on soil arching and the distribution of active earth pressure was experimentally investigated by Pipatpongsa et al. [16]. Guo and Zhou [17] investigated the formation of stable arches in cohesionless granular materials or materials with small apparent cohesion. The results indicated that the material's internal friction angle generally controlled the shape of the arch, while the critical arch width depended on cohesion.

On the other hand, several studies have been carried out using numerical simulations [18-20] and also the Particle Image Velocimetry (PIV) [15, 21-22] to assess the occurrence of arching in granular soils

* Corresponding author. E-mail address: mh.khosravi@ut.ac.ir (M. H. Khosravi).

and to evaluate the expansion of failure in granular materials. PIV was first coined by White et al. [23], who modified the method for application in geotechnical studies. The principles, scope of application, and the mathematical rules governing this method have been studied by many researchers [24]. Some studies have also tried to reduce the error from image processing techniques and to select the appropriate shooting technique [25].

Although many numerical analyses and physical experiments have tried to study the active earth pressure, several other parameters that affect the magnitude of lateral earth pressure on retaining walls require further investigations. In this research, a rigid retaining wall system with the possibility of translation and/or rotation modes was designed and developed. The effect of surcharge pressure on the magnitude and distribution of lateral active earth pressure was investigated. Also, the distribution of earth pressure on the retaining wall was measured utilizing a series of miniature pressure cells. Furthermore, the gradual formation of the failure zone behind the moving wall was studied using the PIV method.



Fig. 1. Physical model box.

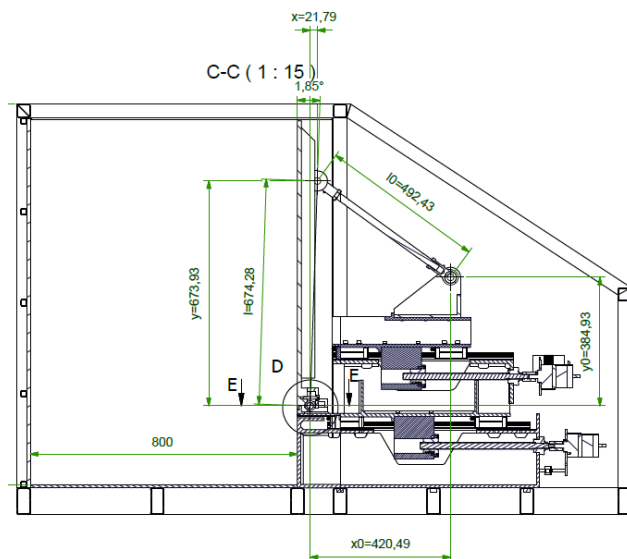


Fig. 2. Schematic image of the physical model.

According to Figure.4, five flat circular miniature pressure cells were mounted inside the pre-embedded holes in the wall at identical intervals. The effective diameter of the pressure cell was about 57 times the average particle size of the backfill. This suggests that the ratio of the particle size to the effective area of pressure cells has been appropriate. The surface of the wall was covered with sandpaper No. 80, except for the face of pressure cells, which provided a rough surface between the soil and the wall. According to the conducted direct shear tests, the

2. Experimental setup and instrumentation

In order to perform the experiments, an acrylic box with metal framing with dimensions of 100 cm height* 80 cm length *31 cm width was designed and constructed according to Figures. 1 and 2. A rigid, thick vertical retaining wall with a height of 85 cm was made inside the box capable of sliding horizontally and/or rotating around the base of the wall.

Figure. 3 illustrates wall motion capabilities. An adjustable linear speed step motor controls each motion mode. The speed of the motors is adjustable and variable from 0.00125 to 0.25mm/s. The magnitude of the wall motion is measured by linear variable differential transformers (LVDT). According to Loukidis and Salgado [26], in retaining walls with a far more considerable length than the width of the backfill, the deformation of the backfill and foundation soil occurs under plane strain conditions.

friction angle of the interaction between the soil and the wall was 90% of the internal friction angle of the soil. In order to read and record the output values of the pressure cells, a data logger with eight analog channels was designed and developed with high precision and simple usability.

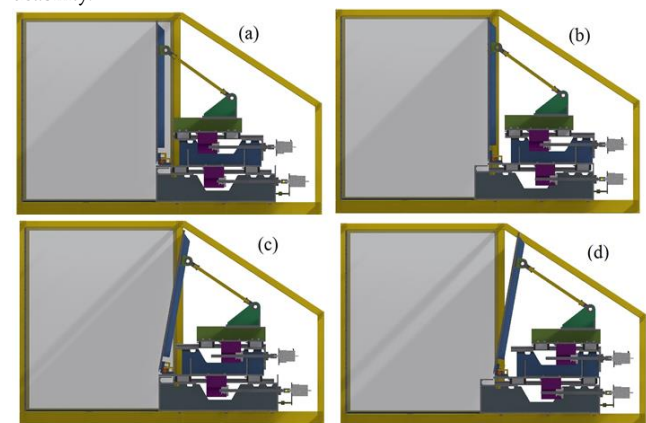


Fig. 3. Schematic design of the box for the physical model (a) The initial conditions of the wall; (b) Translation motion; (c) Rotational motion; (d) Translation-rotational motion.

3. Backfill Specifications

Granular materials used as retained backfills were supplied from Qum Tapa (S1) located in the Eastern Azerbaijan province, 30 km northwest of Tabriz. In addition to purification and relative uniform grading, the main reason for using this type of sand is a high degree of color differentiation. Therefore, according to the concepts presented on

image texture and the particle image velocimetry method, they have an appropriate texture for image processing. In order to separate extra materials, the soil was air-dried and sieved before usage. The physical and mechanical properties of sand were determined through several tests, including sieve analysis, specific gravity, as well as minimum and maximum unit weight determination. A series of direct shear tests were performed on the sand to determine the internal friction angle and the interface friction angles. Based on the Unified Soil Classification System (USCS), the sand was poorly graded. According to Loukidis and Salgado [26], for a very loose backfill, the internal friction angle of the retained backfill is constant during the movement of the wall. Also, all soil components reach the failure limit with a friction angle ϕ equal to the critical state friction angle ϕ_c . Hence, in this study, it is assumed that the internal friction angle of the backfill soil is constant due to the low relative density and the loose backfill. The main characteristics of the utilized materials are presented in Table 1.



Fig. 4. Miniature pressure cells installed in thick rigid wall.

Table 1. Specifications of the utilized sand.

Property	Value	Property	Value
Average particle diameter, D_{50} : mm	0.335	Minimum dry unit weight, kN/m^3	14.60
Uniformity coefficient, C_u	1.6	Maximum dry unit weight (kN/m^3)	17.38
Coefficient of curvature, C_c	1.02	Dry unit weight of experiments kN/m^3	15.68-16.06
Specific gravity, G_s	2.635	Minimum void ratio, e_{min}	0.487
Modulus of elasticity, kN/m^2	24000	Maximum void ratio, e_{max}	0.781
Internal friction angle, ϕ : degrees	33	Void ratio of experiments, e	0.588-0.649
Cohesion, c , kN/m^2	0	Relative density, Dr : %	44.9-65.6

4. Sample preparation process

The sensitivity of pressure cells to the variation in soil stiffness dictates a precise process for developing the model. In this research, the air pluviation method was utilized to fill the box. The nozzle sweep rate, funnel span, fall height, and its increment at each step can be adjusted in the available sand rainer. In order to obtain a uniform density, the dry sand was poured inside the container from a fixed height with a constant speed and rate. Figure 5 reveals the test equipment.

5. Pressure cell calibration

To calibrate the pressure cells, they were installed in a thick metal plate with the same sandpaper that was used for covering the retaining wall. This plate was placed at the bottom of the container. As a seating pressure, a layer of soil was poured on the plate and the surcharge pressure was heightened through a stepwise layering process. Then, the unloading was carried out using vacuum suction, as presented in Figure 6. As the figure shows, the pressure cells reveal an almost linear behavior during the loading process, while their behavior during

unloading is nonlinear. The cause is stress localization around the diaphragm of the pressure cell during the loading and its hysteresis behavior. This behavior of the diaphragm pressure cells in the process of calibration has also been reported by Take & Valsangkar [27] and Khosravi et al. [15].



Fig. 5. Physical model box, sand rainer, and shooting equipment.

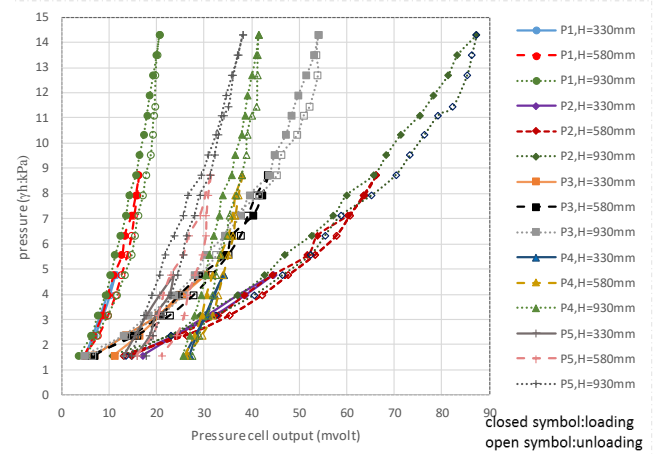


Fig. 6. Loading and unloading process of sand S1.

6. Particle Image Velocity (PIV)

The Particle Image Velocimetry method, as a non-destructive optical procedure, is a very proper, accurate, and inexpensive method for ascertaining the granular soil displacement in geotechnical modeling. In this research, a CANON G10 digital camera with a resolution of 768 x 1024 pixels was used for capturing the images. The images were shot for every 0.092 mm of a horizontal translation (every 60 seconds) by a computer connected to the camera. In order to eliminate the unwanted reflection of light on the chamber and to prevent the occurrence of wild vectors in the analysis of the images due to random lighting changes, a darkroom was set around the box with two 1,000-watt lamps employed on two sides of the camera. Once the shooting was completed, image processing was performed by the GeoPIV program, a MATLAB module developed by Take and White [23].

7. Results and discussion

In this study, a total number of 12 experiments were carried out with the specifications reported in Table 2. All experiments were restricted to the active mode with the linear velocity of both step motors controlling the rotation and translation speed set as 0.00125 mm/s. The output values of the pressure cells were recorded and saved by a data logger with a constant current from the rest conditions to the end of the

experiment. Two LVDTs recorded the motion of the motors by a data logger. In order to investigate the influence of surcharge on the lateral pressure imposed on the soil, various combinations of steel balls with a diameter of 12 to 20 mm were used as a uniform surcharge on the backfill.

Table 2. Specifications of experiments.

Test No.	Motion mode of wall	Wall height, H(mm)	Surcharge, Q (kN/m ²)	Rotation angle (degree)	Active wall movement ($\Delta x_s/H$)
1	Translation	540	0	0	0.006
2		540	0.48607	0	0.0035
3		820	0.718	0	0.006
4		600	1.204	0	0.0035
5	Rotation	812.5	0	3.1	0.006
6		812.5	0.48607	2.67	0.006
7		822.5	0.718	2.9	0.006
8		822.5	1.204	2.82	0.006
9	Translation- Rotation	812.5	0	2.88	0.006
10		812.5	0.48607	2.88	0.006
11		812.5	0.718	2.88	0.006
12		812.5	1.204	3.13	0.006

8. Translation mode

8.1. Lateral earth pressure analysis under the influence of surcharge

Figures 7(a)-(d) demonstrate the changes in the normalized lateral active pressure with the alteration of uniform surcharge during the translation of the wall from the rest condition to the end of the experiment for tests 1 to 4. Also, the profile of the normalized lateral pressure distribution at the wall height is depicted in Figure 8(a-d). In order to compare the experimental results with previous studies, theoretical predictions based on Jaky's at-rest lateral pressure [12], Rankine's active pressure [2], Paik & Salgado (with no surcharge) [5], and Khosravi [13] were also plotted in these profiles. In these diagrams, $\Delta x/H$ represents the normalized cumulative wall horizontal movement from the rest condition, γ is the unit weight of backfill, and H is the height of the backfill. The pressure cell 1 is located at the bottom of the wall. As observed in these diagrams, at the rest condition, i.e., when the wall has no movement, the experimental results show a desirable consistency with Jaky's lateral pressure profile except at the heel of the rigid retaining wall. The cause of partial difference between the measured lateral pressure and Jaky's formulation can be attributed to the preparation process. In physical modeling, the side boundaries of the soil box affect the unit weight of the poured sand. During the soil preparation process, the layer near the vertical boundary of the box, i.e., the adjacency of the wall, has a lower density than other parts. In addition, at the rest condition, a significant decrease in the lateral earth pressure is seen compared to Jaky's lateral pressure at the bottom of the wall. It is owing to the occurrence of local arches caused by slight soil settlement due to the increase in the height of the backfill during the preparation process. The same behavior was reported by Khosravi et al. [15, 28] in their physical and numerical modeling.

By moving the wall in an active translation mode at a constant rate, the values of the lateral pressure of the soil decrease gradually. When the extent of the wall displacement reaches its active value, the normalized lateral pressure values reach their minimum value, after which there is no further considerable decline in the values measured in pressure cells with further rises in the wall translation. Accordingly, the extent of displacement required for obtaining the active state in the experiments was determined and recorded in Table 2. It is observed that in order to obtain the active conditions, the magnitude of active displacement of the wall has been about 0.0035 to 0.006 times the wall height. These values suggest a good agreement with the results reported by Lambe and Whitman [29] and Handy and Spangler [6] for full-size retaining walls. However, they are higher than those proposed in the literature for small-scale laboratory model of retaining walls [15, 30]. The reason can be the effect of scale in miniature models. On the other hand, in the pressure cell installed at the heel of the wall, after the

decline in the recorded value, an increase is observed again. This could be due to the loss of local arches as well as the condition of the backfill adjacent to the boundary of stable and moving parts. The investigation results for the pressure values in the pressure cell installed at the base of the wall reveal that the pressure recorded in the translation active state in surcharges equal to 0, 0.48607, 0.718, and 1.204 kN/m² is 68.55, 64.17, 61.44, and 51.55% of the value calculated by Rankine's equation. Also, examining the diagrams and comparing the results of the physical model with the values predicted by Rankine, it is observed that in contrast to Rankine's equation, the distribution of the lateral active pressure along the wall is nonlinear against depth and it is more consistent with the proposed theoretical relations based on the arching phenomenon. A comparison of the measured active pressure distribution with Rankine's value indicates that the measured value is higher than that of Rankine's solution at the upper parts of the wall and it is lower than Rankine's value at the lower parts of the wall's surface.

In addition, investigating the values read at the stage of active state suggests that these values well match the theories developed by Paik & Salgado [5] and Khosravi et al. [13]. However, in contrast to theory, the amount of lateral pressure at the base of the wall is not reduced to zero. This is related to local arch action at the toe of the wall (see Khosravi et al. [15, 28] for more details). Furthermore, it is seen in figure 8 that by increasing the amount of surcharge, the effect of the arching phenomenon at the base of the wall is more obvious, where the magnitude of pressure increases due to the surcharge in the vicinity of the free surface and the upper half of the wall is higher than the corresponding amount at the base of the wall. Finally, by increasing the surcharge, the pressure recorded at the base of the wall is closer to the predicted values through the theory.

8.2. Deformations Analysis by PIV

The monitoring and analysis of deformations were performed by analyzing the digital images using a MatLab module developed by Take and White [23, 31-32]. The images were recorded every 0.092 mm of a horizontal translation. For analyzing the images, the patch size was chosen as 64 pixels. An example of contours of deviatoric strains and displacement vectors generated during the horizontal translation in test 4 are presented in Figures 9 and 10, respectively. Also, the displacement vectors and contours of deviatoric strains at the time of reaching the active condition in test 1 are provided in Figures 11. It can be deduced from these figures that during the wall active horizontal movement, the distinction between the stationary and failure zones gradually becomes more visible. When the amount of displacement of the wall reaches the level required to achieve the active state, the failure area is completely distinguished from the stationary area. Additionally, multiple nearly parallel shear zones were observed during tests merging in the upper areas of the retaining wall, which then extend to the free boundary of the backfill.

The average angle of the main shear zone relative to the horizon is about 75° in the active condition. As the wall moves beyond the active state, the angle of the main shear zone is reduced to 63° in relation to the horizon. Based on Rankine's equation, which is based on the assumption of the linear distribution of the lateral active pressure behind the wall, in theory, the angle of the failure plane is equal to 61.5° relative to the horizon ($\alpha = \pi/4 + \phi/2 = 61.5$).

However, in physical modeling, this value is rarely obtained where the experimental results in the active state are greater than the theoretical value. This can be attributed to the lateral friction between the soil and the box walls. On the other hand, when the amount of wall displacement is higher than the amount required to obtain the active condition, the angle of the failure plane with the horizon better matches the theoretical results. According to studies, the thickness of the shear zone is a function of the mean diameter of the particle, the pressure level, the initial porosity, as well as grading and roughness of grains [33]. In this study, the shear zone thickness in the wall with the translation motion was about 6.3 mm (approximately 19 times the average particle diameter).

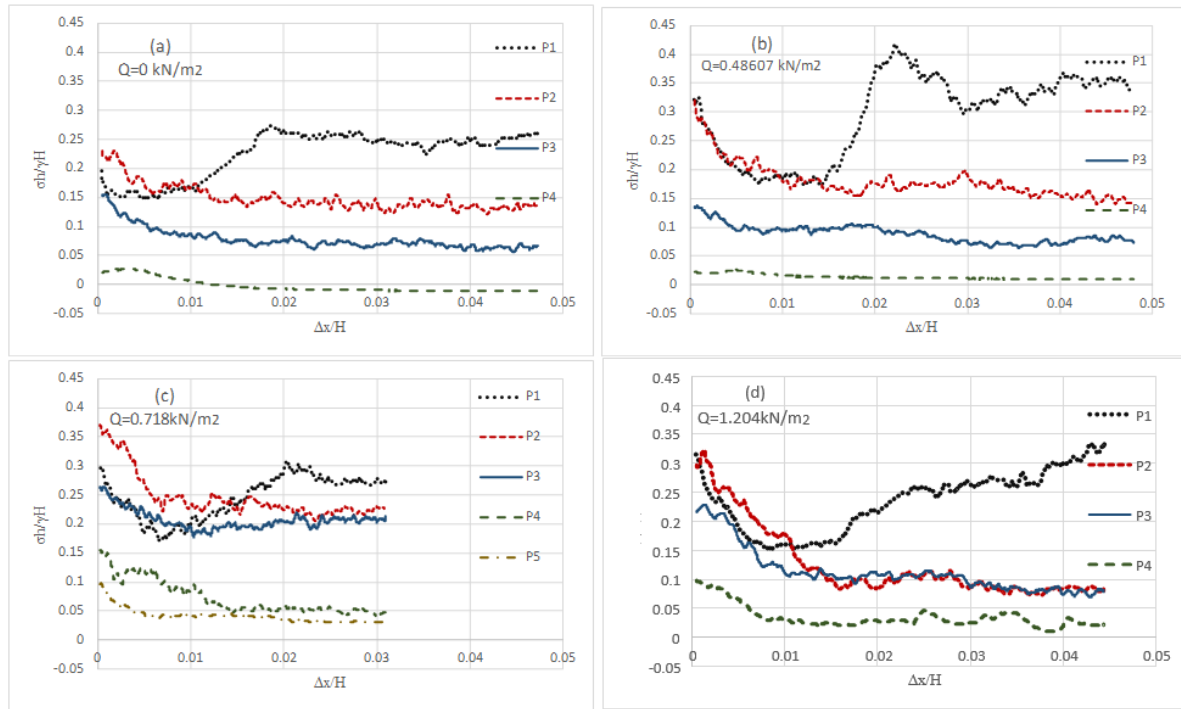


Fig. 7. Changes in the lateral active pressure with alteration of surcharge during the wall translation.

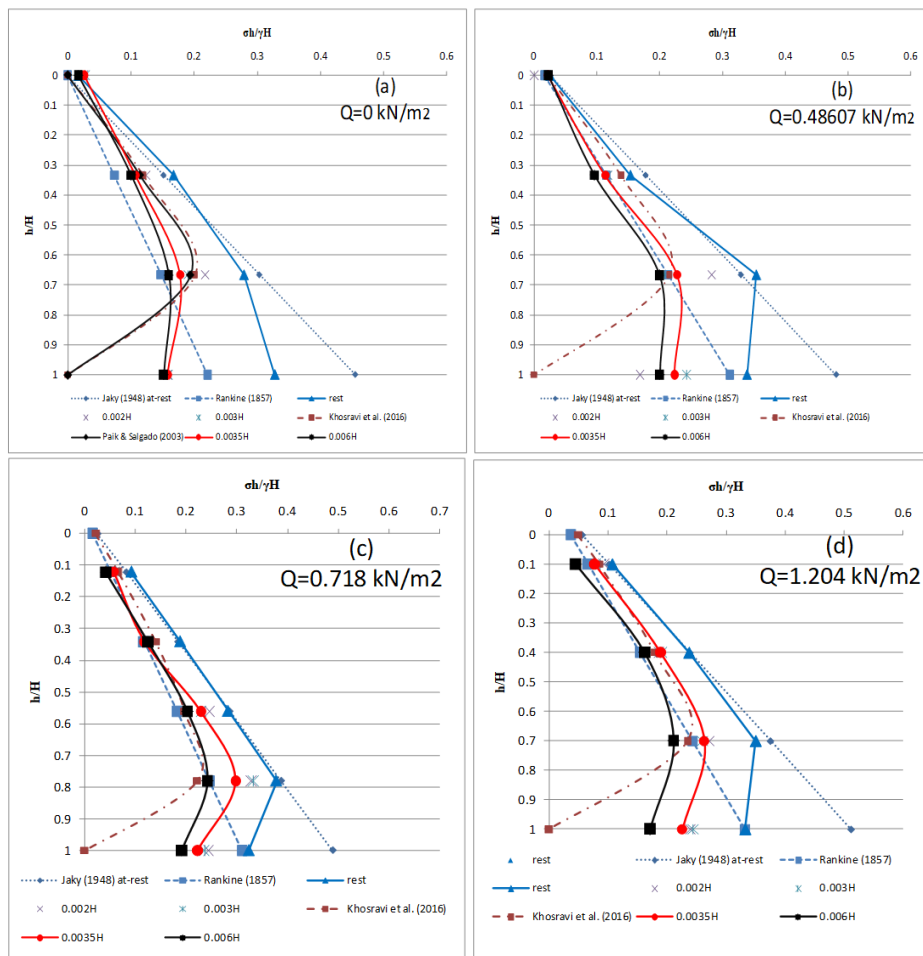


Fig. 8. Distribution of lateral pressure along the wall during the wall translation.

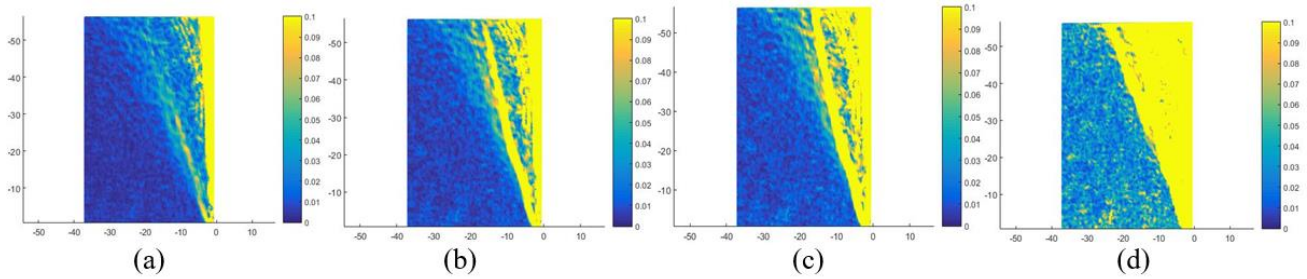


Fig. 9. Contours of deviatoric shear strains generated during the horizontal translation in test 4: $\Delta x/H =$ (a) 0.0035; (b) 0.006; (c) 0.01; (d) 0.03.

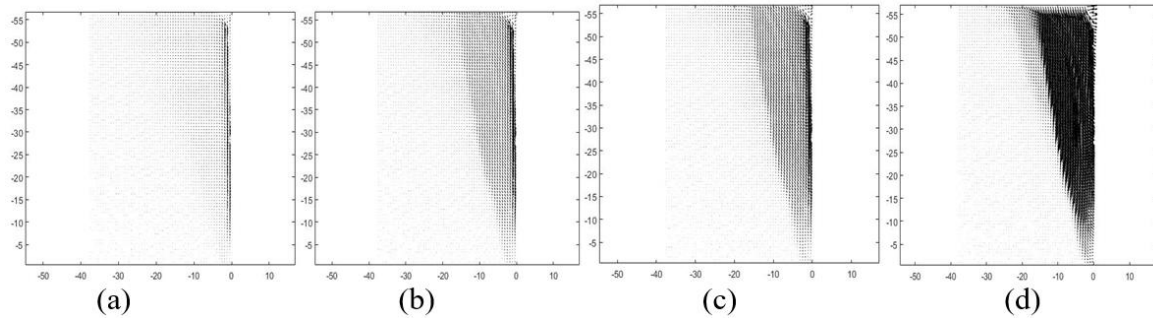


Fig. 10. Displacement vectors generated during the horizontal translation in test 4: $\Delta x/H =$ (a) 0.0035; (b) 0.006; (c) 0.01; (d) 0.03.

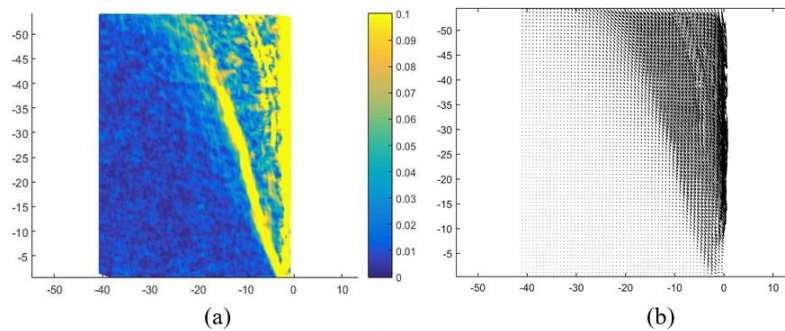


Fig. 11. Displacement vectors (scale=6) and contours of deviatoric strains during the horizontal translation in test 1.

9. Rotation about the base of the wall

9.1. Lateral earth pressure analysis under surcharge

Figures. 12 and 13 display variations in the normalized lateral active earth pressure and the profile of its distribution along the wall height under the influence of variable uniform surcharges during wall rotational motion in tests 5 to 8. In these diagrams, $\Delta x/H$ is the normalized cumulative horizontal displacement of the wall in the upper part from the at-rest condition. As seen in these diagrams, under the rest condition, due to the lack of density of adjacent layer of wall during the preparation process, the laboratory results are about 2 to 8% lower than Jaky's at-rest lateral pressure profile values. On the other hand, due to the formation of local arches and subsidence during construction, this difference becomes more significant at the base of the wall and equates to about 75% of the rest pressure.

Upon the initiation of active rotational motion of the wall, the values of lateral earth pressure gradually decreased and eventually reached a constant value, where no significant changes were observed in the recorded values. The results indicated that in the rotating wall around the base, the pressure variations in the wall height were relatively linear. Also, the pressure values recorded by the pressure cells installed in the

upper part of the wall reached the equilibrium position faster than the other parts, while in the pressure cell installed at the bottom of the wall, the declining process continued and the pressure did not become stable. Since the magnitude of horizontal deformation required to achieve the active condition across all wall heights is relatively constant, this phenomenon at the base of the wall can be predictable. In other words, reaching the active condition at the base of the wall requires a greater amount of rotation while in practice, this is virtually impossible to occur. It can be seen that in general, in order to obtain the active condition, the displacement of the upper part of the wall is about 0.006 times the wall height and is equal to 0.32 degrees. Also, at the displacement value of approximately 0.02 times the wall height (1.1 degrees), the declining rate of pressure at the base of the wall lessens.

In addition, the pressure values recorded at the base of the wall were also investigated. According to the results, the pressure value in the displacement was about 0.006 times the wall height (0.32°) for surcharges equal to 0, 0.48607, 0.718, and 1.204 kN/m² was 81.1, 75.55, 73.01, and 69.19% of the value calculated by Rankine's equation, which is far closer to Rankine's active pressure relative to the translation motion state. Therefore, it can be concluded that the arching phenomenon in the rotational motion around the base of the wall plays a less significant role.

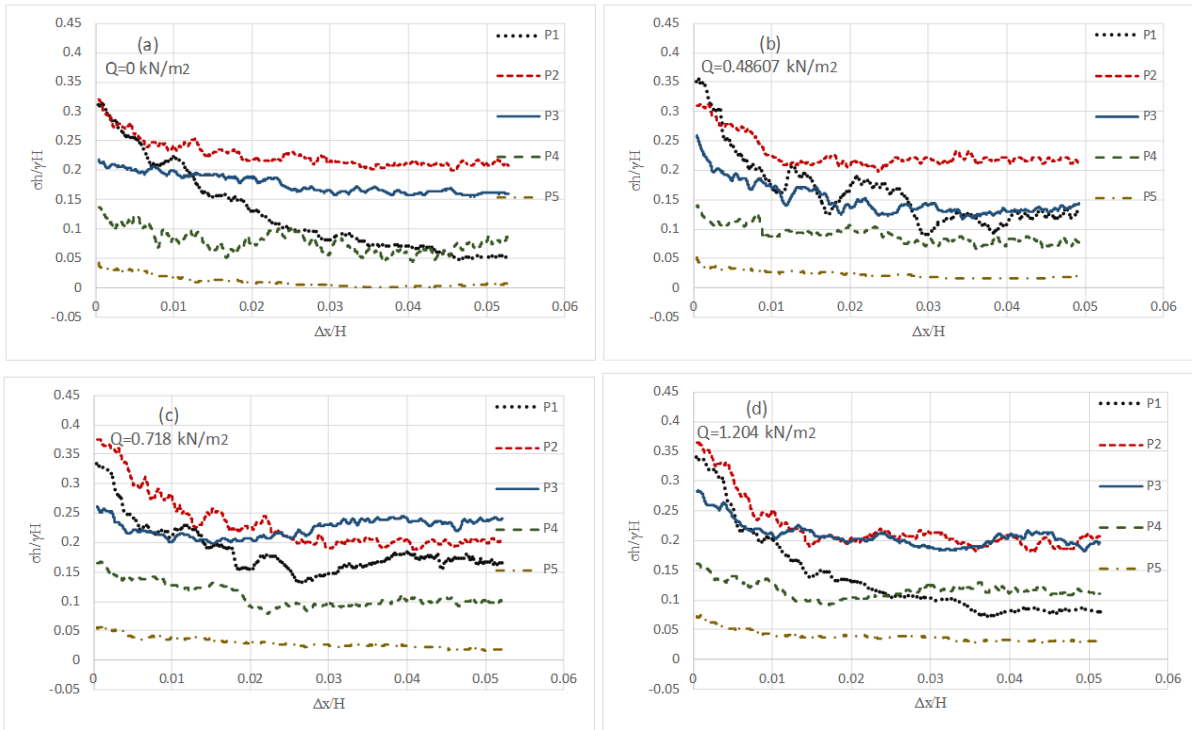


Fig. 12. Changes in the lateral active pressure with alteration of surcharge during the wall rotational motion.

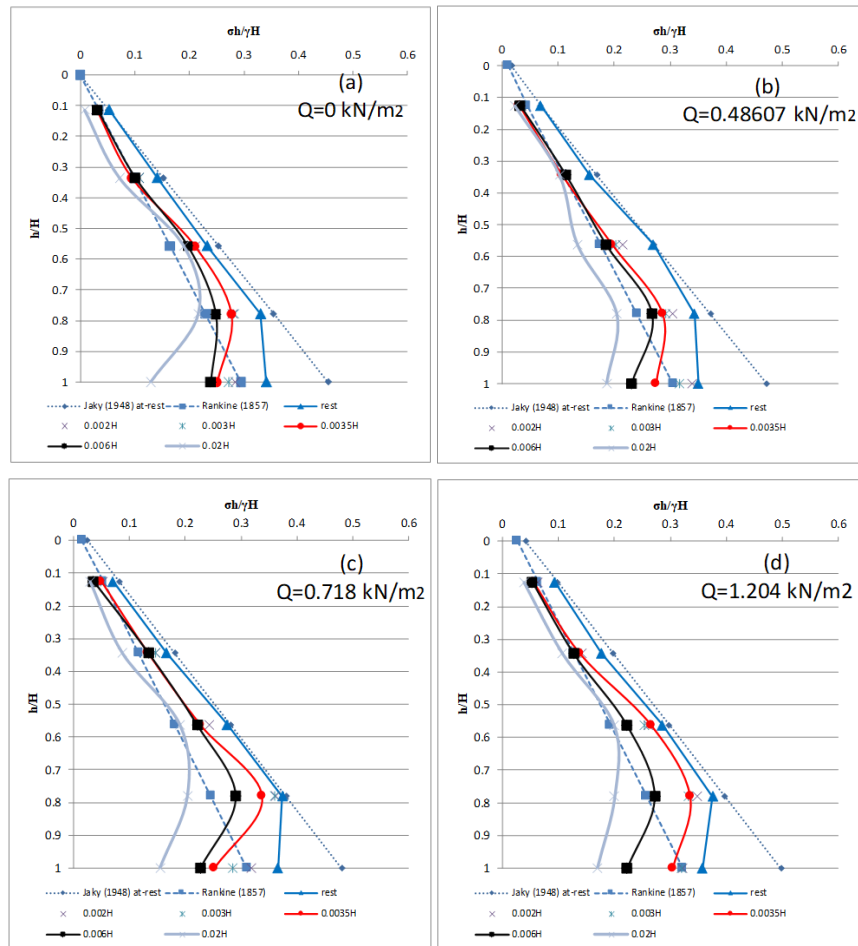


Fig. 13. Distribution of lateral pressure along the wall during the wall rotational motion.

9.2. Deformations Analysis by PIV

Figure. 14 displays an example of displacement vectors and the contours of deviatoric strains at the time of reaching the active conditions under the influence of variable uniform surcharges during the wall rotational motion in test 5. As observed, the failure area includes a series of parallel lines close to each other. The thickness of the shear zone in the rotating wall is less than that of the transitional wall and determined to be about 3.5 mm (about 11 times the average diameter of the particle). Compared to the other investigated modes, the minimum deviatoric strain was considered in this motion mode. The main wedge failure occurs in the upper areas of the wall, which does not expand until reaching the base of the wall.

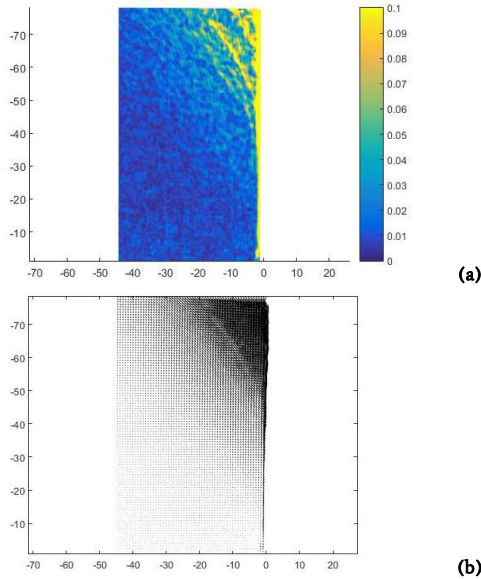


Fig. 14. Displacement vectors (scale 6) and contours of deviatoric strains during the wall rotational motion in test 5.

10. Rotational–translation mode

10.1. Lateral earth pressure analysis under the influence of surcharge

Figures. 15 and 16 demonstrate the changes in the normalized lateral active pressure and the profile of its distribution at wall height under the influence of variable uniform surcharges during wall translation/rotational motion from the rest conditions to the termination of the experiment in tests 9 to 12. According to these diagrams, it is observed that the distribution pattern of active pressure in the translation-rotational motion is more complicated than that of the two previous modes of motion. As the motion commenced, the lateral earth pressure values in pressure cells 2, 4, and 5 gradually decreased and eventually reached a constant value where no significant changes were observed in the recorded values. On the other hand, in the installed pressure cell at the toe of the wall, after reducing the pressure and becoming constant, the ascending trend of recorded values was observed again. Also, in the pressure cell 4, a completely different behavior was observed, where after the growing trend, the diagram reached a constant value. It is seen that generally, for obtaining the active conditions, the displacement of the upper part of the wall has been about 0.006 times the wall height and equal to 0.32 degrees.

In addition, the pressure values recorded at the base of the wall indicated a displacement value of about 0.006 times the wall height (0.32°), for surcharges equal to 0, 0.48607, 0.718, and 1.204 kN/m², it was equal to 61.79, 61.07, 59.07, and 49.7% of the value calculated through Rankine's equation.

10.2. Deformations Analysis by PIV

Fig. 17 presents an example of displacement vectors as well as the contours of deviatoric strains at the time of reaching the active condition with a change in the uniform surcharge value during wall rotational-translation motion in test 9. The shear zone thickness in the rotational-translation moving wall was determined to be 3.3mm (about 10 times the average particle diameter).

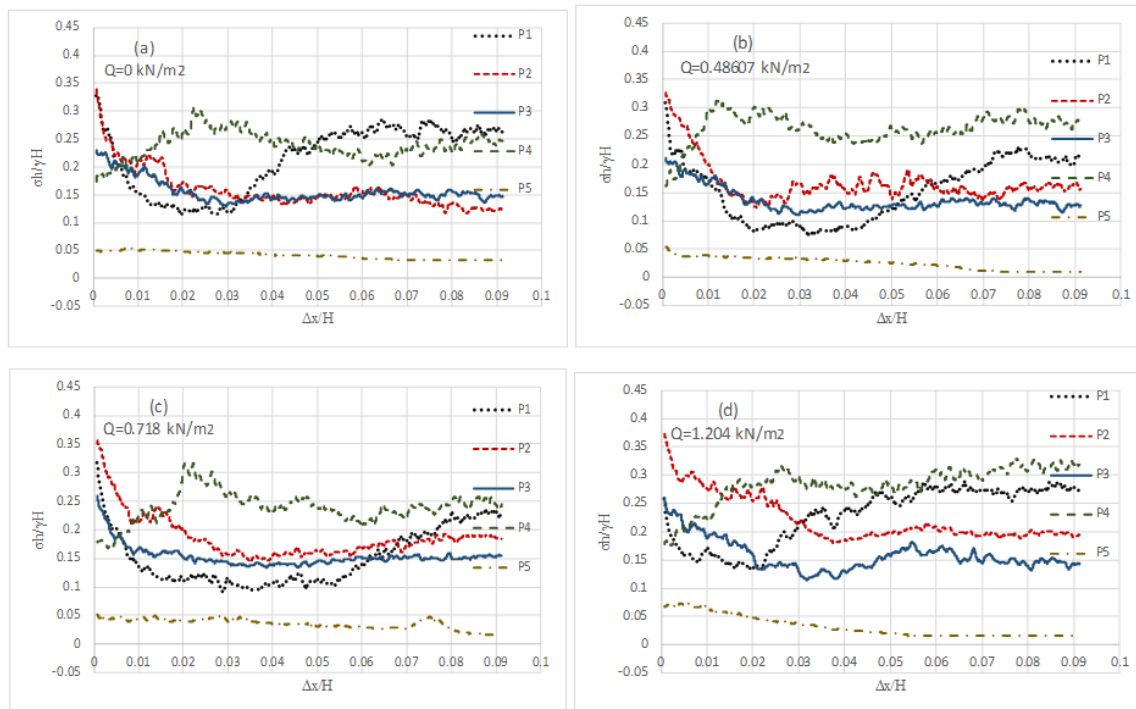


Fig. 15. Changes in the lateral active pressure with the variation of surcharge during the wall translation/rotational motion.

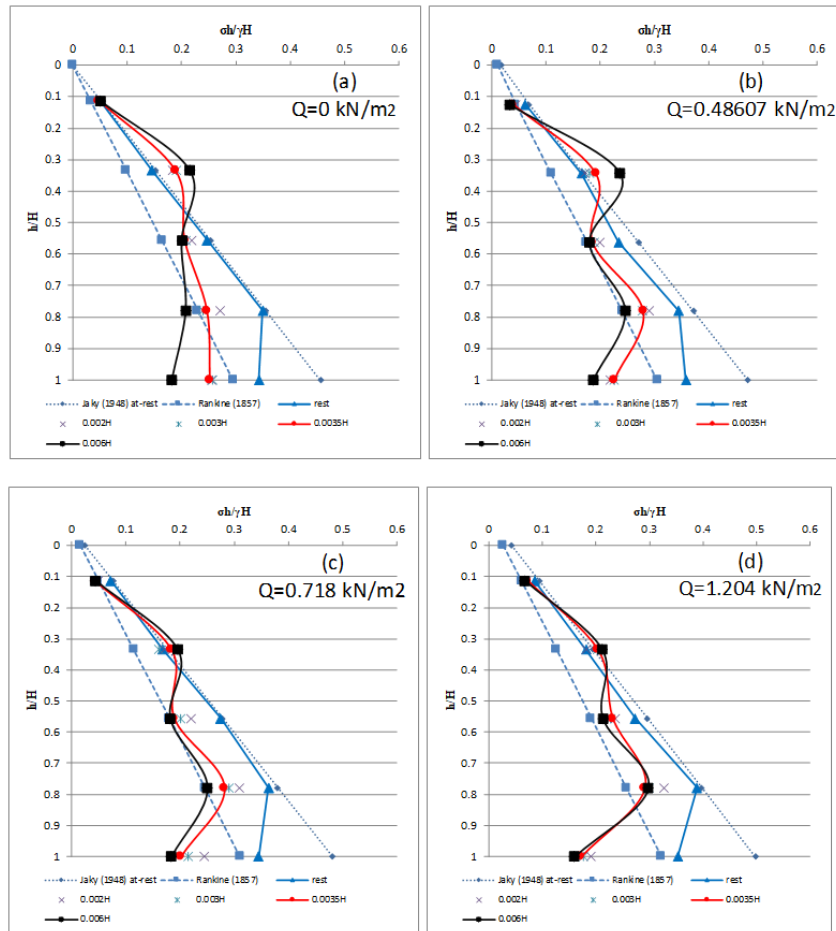


Fig. 16. Distribution of lateral pressure along the wall during the wall translation/rotational motion.

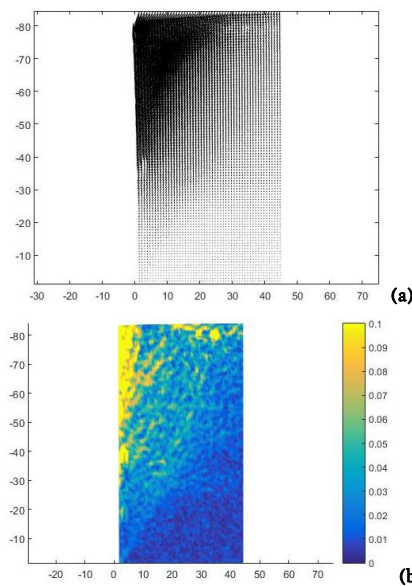


Fig. 17. Displacement vectors (scale 6) and the contours of deviatoric strains during the wall rotational-translation motion in test 9.

11. Conclusions

In order to evaluate the active earth pressure, several physical experiments on a laboratory scale were carried out on a rigid retaining wall with translation, rotational, and translation-rotational motion

modes. Various combinations of steel balls were used as a uniform surcharge on the backfill. In order to investigate the behavior of the soil and the failure wedge, the miniature pressure cells and image analysis (PIV) method were used. The results of the physical experiments of this study were compared with those of theoretical theories developed based on the arching phenomenon. In summary, the results of this study can be concluded as follows.

- Under the at-rest condition of the backfill, experimental results indicated a slight difference with the lateral pressure profile provided by Jaky [12]. The reason for this difference is the manner of model preparation and the low unit weight of the sand adjacent to the lateral borders of the box. At the base of the wall, due to the occurrence of local arches caused by partial settlement of the soil, the difference in the results of the physical and the theoretical model became more visible.

- Upon initiation of the wall active motion, the values of lateral earth pressure gradually decreased and reached its minimum in the active conditions. Afterward, with further movement of the wall, no noticeable reduction was observed in the pressure values recorded in the pressure cells. In order to obtain the active conditions, the active displacement of the wall was about 0.0035 to 0.006 times that of the wall height.

- During the translation and translation/rotational motion, after the reduction of the recorded value by the pressure cell installed at the base of the wall, an ascending trend was observed in the recorded values. This issue could be due to the loss of local arches as well as the state of the backfill adjacent to the stationary base and active part boundary.

- During the translation motion, the distribution of lateral active pressure at the wall height was non-linear in contrast to Rankine's equation. The results were more consistent with the arching-based developed theories. However, unlike the predicted results through the equations, the magnitude of lateral pressure at the base of the wall was

not zero. In general, the values recorded in the upper half of the wall were higher than Rankine's values, while in the lower half, it was less than Rankine's values.

• By increasing the amount of surcharge, the arching effect in the base of the wall became more evident. The amount of pressure increased due to the surcharge in the vicinity of the free surface and the upper half of the wall, which was greater than that of the base of the wall. It seemed that by enhancing the extent of surcharge, the amount of pressure recorded at the base of the wall approached zero.

REFERENCES

- [1] Coulomb, C. (1776). Essai sur une application des regles de maximis et minimis quelques problemes de statique, relatifs a l'architecture. Paris: Memoires de Mathematique de l'Academie Royale de Science 7.
- [2] Rankine, W. J. M. (1857). on the stability of loose earth. Philosophical Transactions of the Royal Society of London, 147, 9-27.
- [3] Janssen, H. A. (1985). Versuche uber Getreidedruck in Silozellen. Aeitsc hri fi, Verein Deutscher Ingenieure, 39, 1045-1049.
- [4] Terzaghi, K. (1943). Theoretical soil mechanics. New York(NY): John Wiley & Sons.
- [5] Paik, K. H. & Salgado, R. (2003). Estimation of active earth pressure against rigid retaining walls considering arching effects. *Geotechnique*, 53(7), 643–653.
- [6] Handy, R. & Spangler, M. (2007). Geotechnical Engineering: Soil and Foundation Principles and Practice. 5 ed. s.l.:McGraw-Hill Education.
- [7] O'Neal, T. & Hagerty, D. (2011). Earth pressures in confined cohesionless backfill against tall rigid walls — a case history. *Canadian Geotechnical Journal*, 48(8), 1188–1197.
- [8] Iskander, M. et al. (2013). Active static and seismic earth pressure for $c-\phi$ soils. *Soils and Foundation*, 53(5), 639–652.
- [9] Khosravi, M. H. (2012). Arching effect in geomaterials with applications to retaining walls and undercut slopes. PhD dissertation, Department of International Development Engineering, Graduate School of Science and Engineering, Tokyo Institute of Technology.
- [10] Khosravi, M. H., Kargar, A. R., & Amini, M. (2018). Active earth pressures for non-planar to planar slip surfaces considering soil arching. *International Journal of Geotechnical Engineering*. DOI: 10.1080/19386362.2018.1503439.
- [11] Pipatpongsa, T. & Heng, S. (2010). Granular arch shapes in storage silo determined by quasi-static analysis under uniform vertical pressure. *Journal of Solid Mechanics and Materials Engineering*, 4(8), 1237-1248.
- [12] Jaky, J. (1948). Earth pressure in silos. *Soil Mechanics and Foundation Engineering*, London, 103–107.
- [13] Khosravi, M., Pipatpongsa, T. & Takemura, J. (2016). Theoretical analysis of earth pressure against rigid retaining walls under translation mode. *Soils and Foundations*, 56(4), 664–675.
- [14] Khosravi, M. H., Bahaaddini, M., Kargar, A. R., & Pipatpongsa, T. (2018). Soil Arching Behind Retaining Walls under Active Translation Mode: Review and New Insights. *International Journal of Mining and Geo-Engineering*, 52(2), 131-140
- [15] Khosravi, M. H., Pipatpongsa, T. & Takemura, J. (2013). Experimental analysis of earth pressure against rigid retaining walls under translation mode. *Geotechnique*, 63(12), 1020–1028.
- [16] Pipatpongsa, T., Khosravi, M. H., & Takemura, J. (2014). Physical model of a rigid retaining wall under translation mode and its variation of arch action in backfill material with interface friction. The 8th International Conference on Physical Modelling in Geotechnics, Perth, Australia.
- [17] Guo, P. & Zhou, S. (2013). Arch in granular materials as a free surface problem. *International Journal for Numerical and Analytical Methods in Geomechanics*, 37(9), 1048–1065.
- [18] Srinivasa, S. & Radoslaw, L. M. (2012). Arching in Distribution of Active Load on Retaining Walls. *Journal of Geotechnical and Geo-Environmental Engineering*, 138(5), 575–584.
- [19] Krabbenhoft, K. (2017). OptumG2: Theory, Optum Computational Engineering. Available at: www.optumce.com
- [20] Krabbenhoft, K. (2018). Static and seismic earth pressure coefficients for vertical walls with horizontal backfill. *Soil Dynamics and Earthquake Engineering*, 104, 403–407.
- [21] Lesniewska, D. & Wood, D. M. (2009). Observations of Stresses and Strains in a Granular Material. *Journal of Engineering Mechanics*, 135(9), 1038-1054.
- [22] Niedostatkiewicz, M., Lesniewska, D. & Tejchm, J. (2011). Experimental Analysis of Shear Zone Patterns in Cohesionless for Earth Pressure Problems Using Particle Image Velocimetry. *Srain*, 47(s2).
- [23] White, D. J., Take, W. A. & Bolton, M. D. (2003). Soil deformation measurements using particle image velocimetry (PIV) and photogrammetry. *Geotechnique*, 53(7), 619–631.
- [24] Raffel, M., Willert, C., Wereley, S. & Kompenhans, J. (2007). Particle Image Velocimetry. A Practical Guide. Second Edition ed. s.l.:Springer .
- [25] Higham, J. & Brevis, W. (2019). When, what and how image transformation techniques should be used to reduce error in Particle Image Velocimetry data?. *Flow Measurement and Instrumentation*.
- [26] Loukidis, D. & Salgado, R. (2012). Active pressure on gravity walls supporting purely frictional soils. *Canadian Geotechnical Journal*, 49(1), 78–97.
- [27] Take, W. A. & Valsangkar, A. J. (2001). Earth pressures on unyielding retaining walls of narrow backfill width. *Canadian Geotechnical Journal*, 38(6), 1220–1230.
- [28] Khosravi, M. H., Hamed Azad, F., Bahaaddini, M., & Pipatpongsa, T. (2017). DEM Analysis of Backfilled Walls Subjected to Active Translation Mode. *International Journal of Mining & Geo-Engineering* 51 (2), 191-197.
- [29] Lambe, T. W. & Whitman, R. V. (1969). Soil mechanics. New York: John Wiley & Sons.
- [30] Fang, Y. & Ishibashi, I. (1986). Static earth pressures with various wall movements. *Journal of Geotechnical Engineering*, 112(3), 317–333.
- [31] White, D. J., Randolph, M. & Thompson, B. (2005). An image-based deformation measurement system for the geotechnical centrifuge. *International Journal of Physical Modelling in Geotechnics*, 5(3), 1-12.
- [32] White, D. J. & Take, W. A. (2003). GeoPIV, 7.6 ed., Cambridge, UK: Cambridge University Engineering Department.

- [33] Tejchman J. (2008). Deterministic and statistical size effect during shearing of granular layer within a micro-polar hypoplasticity. *International Journal for Numerical and Analytical Methods in Geomechanics*, 32, 81–107.